RSC Advances

PAPER

View Article Online
View Journal | View Issue

Cite this: *RSC Adv.*, 2026, **16**, 30916

A high surface area silica-supported aldehyde as a flow-compatible amine scavenger

A. Michelle Reinhardt, [ab] Jenny-Lee Panayides *[b] and Darren L. Riley *[a]

Received 26th May 2026
Accepted 27th May 2026

DOI: 10.1039/d6ra04582k

rsc.li/rsc-advances

A silica-supported aldehyde scavenger (**SSA-3**) was prepared from **SBA-15** silica by sequential NaOH activation, alkylation with 1,2-dichloroethane, and Kornblum oxidation of the resulting alkyl chloride in DMSO/K_2CO_3. The material was characterised by FTIR, PXRD, TGA/DSC, SEM, and BET physisorption, confirming successful surface functionalisation and a dramatic increase in surface area upon imine formation with probe amines. Loading capacity was experimentally determined to be 0.43–1.31 mmol g^{-1}, comparable to commercial polystyrene-aldehyde resins. A D-optimal design of experiments (22 runs) evaluated the effects of solvent type (mapped by PCA), flow rate (0.1–1.0 mL min^{-1}), temperature (30–90 °C), and amine concentration (0.2–1.0 M) on scavenging efficiency. Only solvent type had a significant influence on performance: hydrophobic solvents afforded near-quantitative scavenging, while polar non-polarisable solvents (notably acetonitrile) reduced efficiency to approximately 75% due to a solvation screening mechanism. The scavenger is flow-compatible and demonstrates utility as an in-line purification tool for continuous flow synthesis of small-molecule libraries.

Introduction

Solid-supported reagents (SSRs) occupy an important niche in modern synthetic chemistry, enabling simplified work-up through catch-and-release and scavenging strategies and lending themselves naturally to integration within continuous flow platforms.[1,2] Among the most broadly applicable SSR applications is the removal of excess amines — substrates that are challenging to purge by conventional liquid–liquid extraction owing to their basicity, water solubility, and propensity for silica gel retention.[3]

Commercially available amine scavengers fall into two broad categories. Reversible, ion-exchange-type scavengers (*e.g.* sulphonic acid resins, Dowex 50WX2) operate through protonation of the amine and are broadly selective, capturing primary, secondary, and tertiary amines.[4] Irreversible, covalent scavengers—including solid supported acid chlorides, aldehydes, and isocyanates—react to form stable amide, imine, or urea bonds, respectively, but are selective for primary and secondary amines only.[5–8] Although commercial SS aldehydes and isocyanates are available, they remain expensive relative to the base materials required for their synthesis, and sourcing them can still be problematic.[9,10]

The Kornblum oxidation – in which an alkyl halide is oxidised to an aldehyde by DMSO under basic conditions – offers a mild and operationally simple route to surface-bound aldehydes from readily available alkyl-halide-functionalised supports.[11] Jal and co-workers demonstrated that **SBA-15** silica can be directly alkylated following base deprotonation of surface silanols, without recourse to conventional silane linkers like 3-(trimethoxysilyl) propylamine.[12] The use of silica as an SSR support offers several advantages relative to polymer-based supports: reduced production cost, absence of swelling behaviour, superior structural rigidity, and more favourable diffusion characteristics.[13,14]

Building on this precedent and wishing to develop an affordable amine scavenger that was amenable for use in a flow-based platform, we adapted the methodology by Jal and co-workers[12] for the preparation of a silica-supported aldehyde (**SSA-3**) from **SBA-15** *via* a three-step sequence. The physicochemical characterisation, chemical modification, determination of loading capacity, and a systematic design of experiments (DoE) study of its scavenging performance under continuous flow conditions is reported herein.

Results and discussion

SSA-3 was prepared in three steps from **SBA-15** silica (Scheme 1). Silica was first refluxed in aqueous NaOH overnight to deprotonate surface silanol groups, and water was removed *in vacuo* to afford **SSA-1** as a hygroscopic glass-like solid. **SSA-1** was subsequently alkylated by reflux in 1,2-dichloroethane to install a surface chloroethyl ether (**SSA-2**), and the terminal chloride was oxidised to the corresponding aldehyde by heating in DMSO in the presence of catalytic potassium carbonate at 120 °C for 48 h (Kornblum oxidation), affording **SSA-3**.[11]

[a]*University of Pretoria, South Africa. E-mail: darren.riley@up.ac.za*
[b]*Council for Scientific and Industrial Research, South Africa. E-mail: jpanayides@csir.co.za*

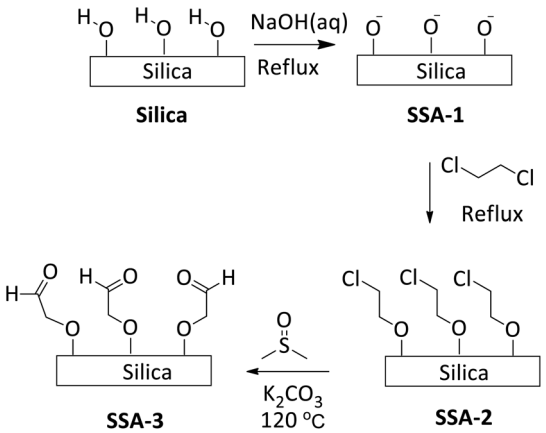

Scheme 1 Synthetic preparation of **SSA-3**.

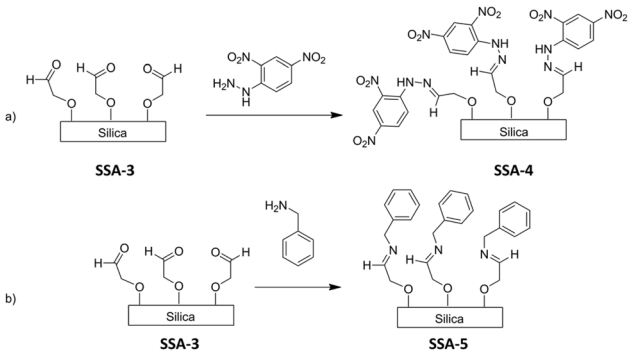

Scheme 2 Chemical derivatisation of **SSA-3** with DNPH (a) and benzyl amine (b).

Successful aldehyde functionalisation was initially suggested qualitatively through reaction with 2,4-dinitrophenylhydrazine (DNPH) solution, which afforded **SSA-4** as a dark orange powder consistent with imine formation (Scheme 2a; Fig. 1). In contrast, unfunctionalised silica treated with DNPH under identical conditions (**SSA-7**) did not show a notable colour change, confirming that the colour response was attributable to the covalently installed aldehyde rather than surface adsorption. In addition, **SSA-3** was also treated with excess benzylamine at ambient temperature over one-week to afford **SSA-5** which as expected showed no distinctive colour change but was prepared as an exemplar to be subjected to physical characterisation (Scheme 2b). In addition, pure silica was also treated with DNPH and benzyl amine to afford **SSA-6** and **SSA-7** respectively which served as negative controls. **SSA-3** could be stored for several months in a desiccator under an argon atmosphere.

Physical characterisation

Samples **SSA-3** to **SSA-7** and unfunctionalised silica were then subjected to BET physisorption, particle size distribution, PXRD, TGA/DSC, FTIR, and SEM analysis. **SSA-1** and **SSA-2** were excluded from physical characterisation owing to their hygroscopic nature.

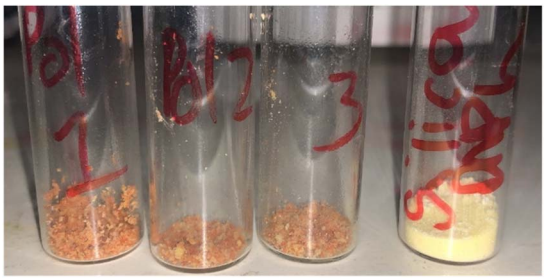

Fig. 1 Photograph of qualitative DNPH test with oxidized silica **SSA-4** (repeats 1-3) with the silica-DNPH **SSA-7** (control, right).

FTIR analysis

FTIR analysis confirmed the presence of the organic linker in **SSA-3**, evidenced by the appearance of C–C bending mode at 1395 cm^{-1} and a carbonyl stretch at 1746 cm^{-1}. The characteristic Si–O–Si stretching modes at 1038 and 1120 cm^{-1} (asymmetric) and 855 and 880 cm^{-1} (symmetric) were preserved across all samples, confirming the integrity of the silica backbone (Fig. 2B). We initially had concerns as the carbonyl stretch is at the upper end of the expected range for an aliphatic aldehyde, arguably extending into the range expected for esters and lactones. That being noted, subsequent reaction with DNPH and benzyl amine to afford **SSA-4** and **SSA-5** showed the characteristic C=N stretch at 1740 cm^{-1} (Figure 2D) and 1738 cm^{-1} (Fig. 2C) respectively, supporting the assignment of the 1746 cm^{-1} in **SSA-3**. In addition, **SSA-5** also showed a C=C stretching mode at 1447 cm^{-1} attributable to the benzyl ring (Fig. 2).

BET physisorption

BET physisorption isotherms (Fig. 3) revealed a modest increase in surface area from unfunctionalised silica (1.27 m^2 g^{-1}) to

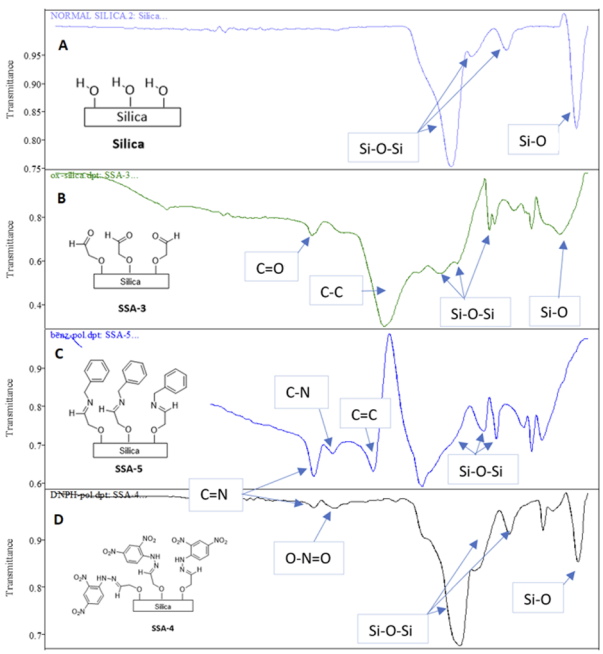

Fig. 2 FTIR transmittance spectra: (A) – **SBA-15** silica, (B) – **SSA-3**, (C) – **SSA-5** and (D) **SSA-4**.

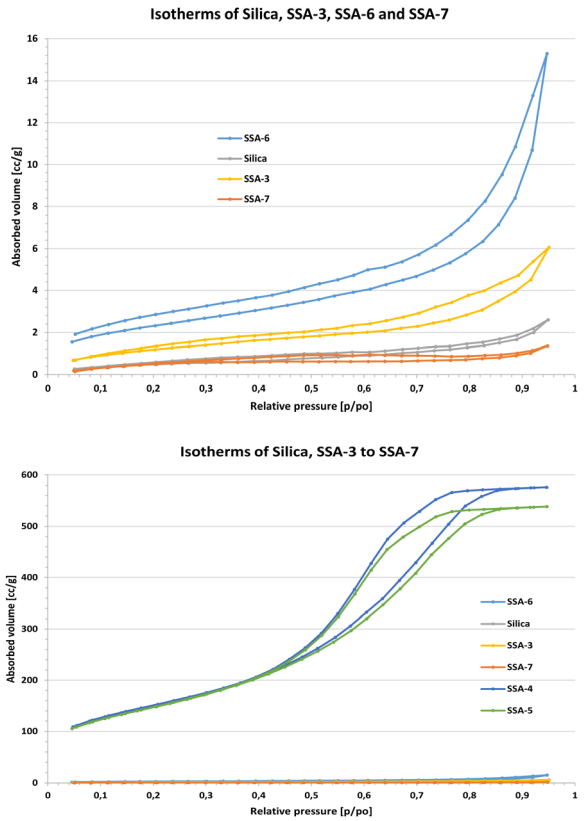

Fig. 3 Top: overlays of Isotherms SSA-3 to SSA-7 and silica; bottom: overlays of isotherms for silica, SSA-3, SSA-6 and SSA-7.

SSA-3 (3.05 $m^2\ g^{-1}$), consistent with surface modification. Strikingly, covalent modification of **SSA-3** with DNPH (**SSA-4**) and benzylamine (**SSA-5**) resulted in 140- and 135-fold increases in surface area relative to **SSA-3**, reaching 424 and 413 $m^2\ g^{-1}$ respectively (Table 1). This was mirrored by an increase of ~124 fold in the monolayer capacity for both **SSA-4** and **SSA-5**, indicating the formation of pseudo-pores among the coupled groups leading to a significant increase in available surface for gas adhesion. Both materials exhibited type IV isotherms (See SI for additional figures) with H2(b) hysteresis, indicative of disordered pore structures with a mixture of mesopores and micropores, in contrast to the H3 hysteresis of the parent silica and **SSA-3** which only have slit-like mesopores with no evidence of micropores (Table 1). The silica controls **SSA-6** and **SSA-7**, formed by reacting unfunctionalised silica with benzylamine and DNPH respectively, showed no significant increase in surface area, confirming that the surface area enhancement is a consequence of covalent modification of **SSA-3** rather than simple adsorption.

The increase in the surface area upon imine formation is attributed to a physical change in pore geometry rather than a measurement artefact: the transition from H3 to H2(b) hysteresis and the appearance of micropores in **SSA-4**/**5** that are absent in **SSA-3** and the silica controls indicate that the surface-confined imine layer introduces *de novo* microporosity through the geometry of the packed organic monolayer at the silica surface.

Particle size distribution

Particle size distribution (Fig. 4) was obtained by plotting the derivative of pore volume as a function of half pore width (derived from BET analysis). In silica and **SSA-3**, pores with half widths up to 7.8 nm are responsible for gas adsorption, in contrast in **SSA-4** and **SSA-5** a spike in gas adsorption occurs between 1–3.8 nm half pore width beyond which no other pore sizes are seen to be absorbing gas in significant amounts. The curves of silica and **SSA-3** shows similar size distributions whereas both covalent modifications **SSA-4** and **SSA-5** show significantly increased absorption at low pressures ($P/P_0 < 0.3$), which can be attributed of the presence of micropores that are absent in silica and **SSA-3**. That being noted **SSA-4** and **SSA-5** also show mesopores in the range of 2–4 nm.

PXRD analysis

PXRD patterns were recorded primarily as reference spectra to facilitate quality control by independent preparers of **SSA-3**. The parent **SBA-15** silica is amorphous by PXRD; the appearance of peaks at 25–30° 2θ following surface functionalisation is attributable to the organic layer and serves as a fingerprint for successful modification (Fig. 5). Both **SSA-4** and **SSA-5** retained crystalline character (25–45° 2θ), while **SSA-7** remained amorphous. **SSA-6** displayed a crystalline morphology which was attributed to masking of the underlying amorphous silica signal by the surface-bound benzylamine layer.

TGA/DSC analysis

TGA/DSC analysis of **SSA-3** showed a 13.62% mass loss below 150 °C attributed to residual solvent, two mass loss events

Table 1 Summary of BET results

Code	Description	S_{BET} ($m^2\ g^{-1}$)	Half pore width (nm)	V_p ($cm^3\ g^{-1}$)	Monolayer capacity ($cm^3\ g^{-1}$)	Isotherm and hysteresis type[a]	Pore type
Silica	Silica	1.2718	1.3236	0.0032	0.385	IV, H3	Meso
SSA-3	Oxidized silica	3.0479	1.3845	0.0079	1.06	IV, H3	Meso
SSA-4	Oxidized silica DNPH	424.2920	2.2713	0.8493	124.73	IV, H2(b)	Meso and micro
SSA-5	Benzylated oxidized silica	412.7466	2.2713	0.7920	124.38	IV, H2(b)	Meso and micro
SSA-6	Benzylated silica	7.2252	3.8976	0.0194	0.640	IV, H3	Meso
SSA-7	Silica DNPH	1.0381	1.2097	0.0016	0.691	IV, H4	Meso

[a] Classified according to the IUPAC classification guideline.

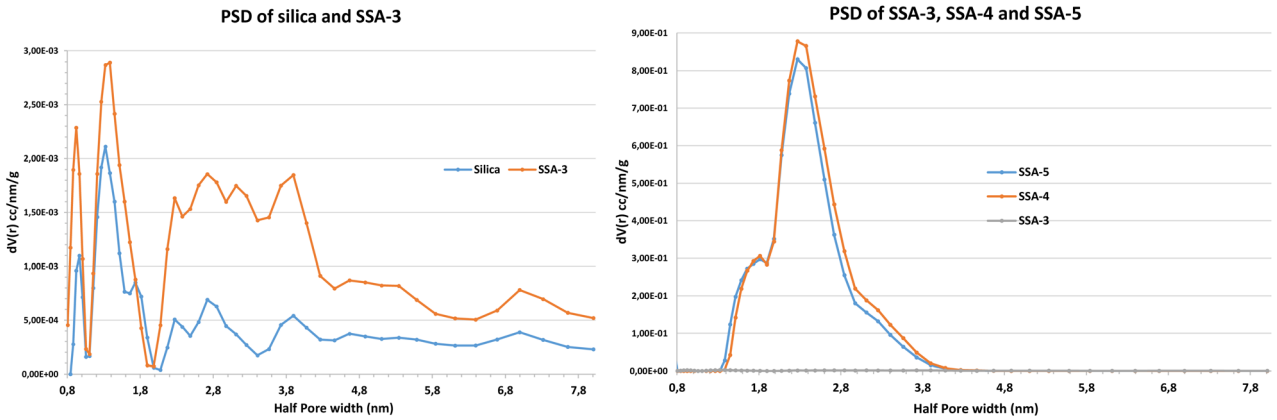

Fig. 4 PSD curves of silica and **SSA-3** (left); and **SSA-3**, **SSA-4** and **SSA-5** superimposed (right).

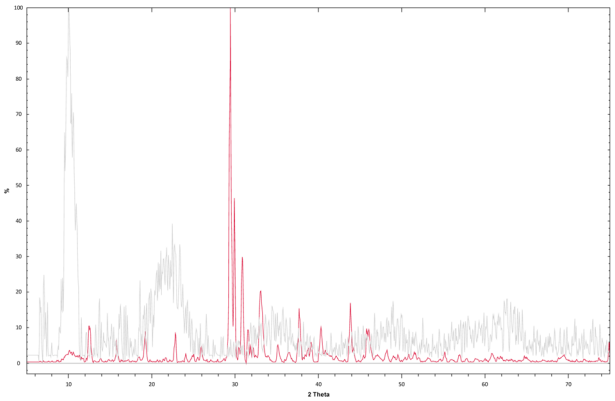

Fig. 5 PXRD overlay of Silica (grey) and oxidized silica **SSA-3** (red) (see SI for additional PXRDs).

between 170–205 °C (combined 10.42% loss) consistent with decomposition of the organic surface functionality, and a final combustion event at 736 °C. Silica controls showed only moisture loss below 150 °C and a high-temperature mass loss event, with no intermediate decomposition (Fig. 6 and Table 2). The distinct thermal profiles of **SSA-4** and **SSA-5** relative to their silica controls (**SSA-7** and **SSA-6**) further corroborated the successful and structurally distinct surface modification of **SSA-3** (Fig. 7 and Table 2).

SEM imaging

SEM imaging confirmed a striking morphological change upon surface oxidation: unfunctionalised silica displayed a smooth, non-porous surface, while **SSA-3** presented a highly porous, rough surface with a spherical aggregate morphology. Following imine formation, **SSA-4** displayed a 'cauliflower-like' granular surface texture with homogeneous roughness, consistent with uniform surface growth. **SSA-7** (silica control treated with DNPH) retained the smooth morphology of unfunctionalised silica (Fig. 8).

Chemical characterisation

Partition test. To confirm that **SSA-3** retains amines by covalent bond formation rather than by reversible chromatographic partitioning, a continuous flow partition test was conducted using *N*-benzylamine (0.2 M in isopropanol, 2.0 mL plug) pumped through an **SSA-3** packed bed (8.1 mL column, 0.1 mL min^{-1}, 30 °C, 8 bar) (Scheme 3). The flow stream was collected in 2.0 mL increments over a collection window of 4.0 to 8.0 mL (Fig. 9). No benzylamine elution was detected in the

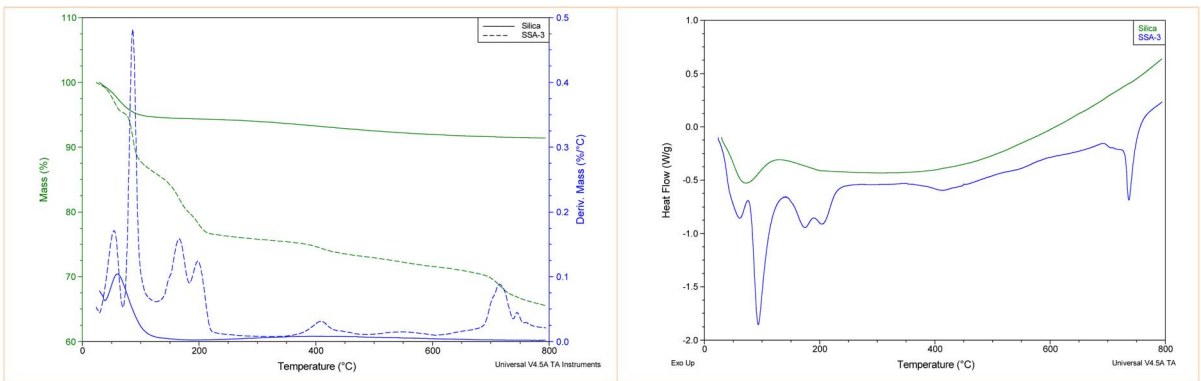

Fig. 6 TGA (green) and DTA (Blue) curves for silica and **SSA-3** (left) and DSC curves (right) for silica (green) and **SSA-3** (blue).

Table 2 Summary of significant events for TGA, DTG and DSC results

	Ranges of significant events (°C)		
Code	TGA	DTG	DSC
Silica	<150	<150	<150
SSA-3	<150, 150–205, 697–800	<150, 173.81, 203.9, 736.47	<150 (endo), 173.81 (endo), 203.9 (endo), 736.47 (endo)
SSA-4	<160, 600–720	<160, 400, 600–720	114.10 (endo), 719.79 (endo)
SSA-5	<150, 150–205, 700–800	<150, 173.81, 737.0	<150 (endo), 173.81 (endo), 737.0 (endo)
SSA-6	<150, 150–205, 700–800	<150, 171.66, 199.63, 736.47	<150 (endo), 171.66 (endo), 199.63 (endo), 736.47 (endo)
SSA-7	<150, 700–800	<150, 741.31	<150 (endo), 741.31 (endo)

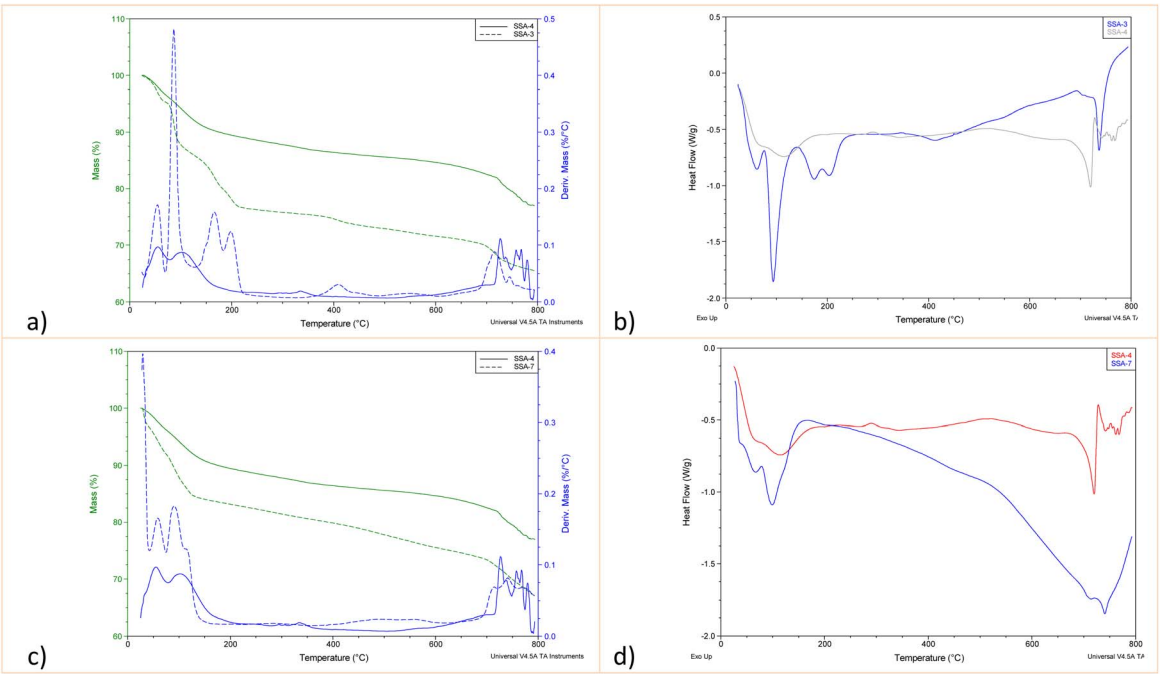

Fig. 7 Overlays of: (a) TGA (green) and DTA (blue) traces of oxidized silica-DNPH **SSA-4** (solid line) and oxidized silica **SSA-3** (dashed line), (b) DSC traces of oxidized silica-DNPH **SSA-4** (grey) and oxidized silica **SSA-3** (blue), (c) TGA (green) and DTA (blue) traces of oxidized silica-DNPH **SSA-4** (solid line) and silica-DNPH **SSA-7** (dashed line), (d) DSC traces of oxidized silica-DNPH **SSA-4** (red) and silica-DNPH **SSA-7** (blue).

expected range of 6–8 mL (red dashed lines). To ensure that we had not cut off the elution too early we next repeated the test using spent **SSA-3** (*i.e.* **SSA-5**), under these conditions *N*-benzylamine could not covalently bond and was eluted between 6.0 and 8.0 mL as expected (Fig. 10). Silica alone under identical conditions showed elution of benzylamine between 14–16 mL by partitioning (Fig. 10).

Loading capacity. Loading capacity was determined by repeatedly injecting benzylamine solution through the same **SSA-3** column under partition test conditions. The percentage amine not absorbed remained below 2% for the first seven runs, and thereafter increased sharply in runs 8 and 9, indicating the onset of saturation (Fig. 11). Combining the absorbed amine from the initial partition test and nine loading capacity runs,

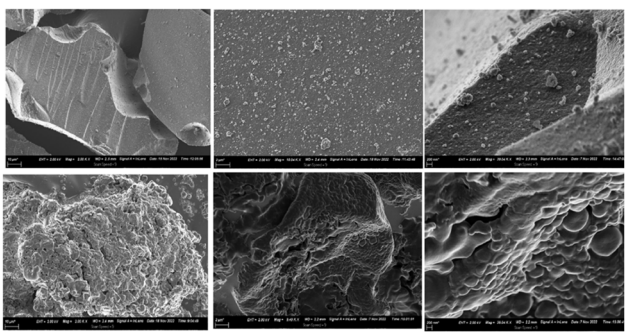

Fig. 8 SEM images of silica (top row) and **SSA-3** (bottom row) at different magnifications.

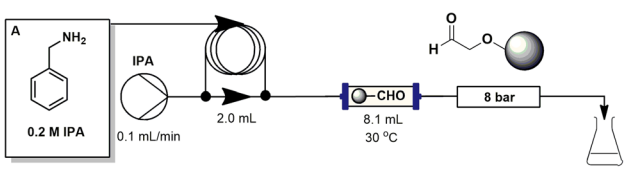

Scheme 3 Flow reactor setup for the **SSA-3** partition test.

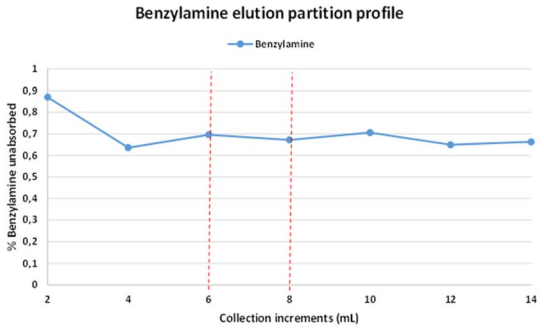

Fig. 9 Elution profile of partition profile run 1, red dotted lines indicate expected elution zone.

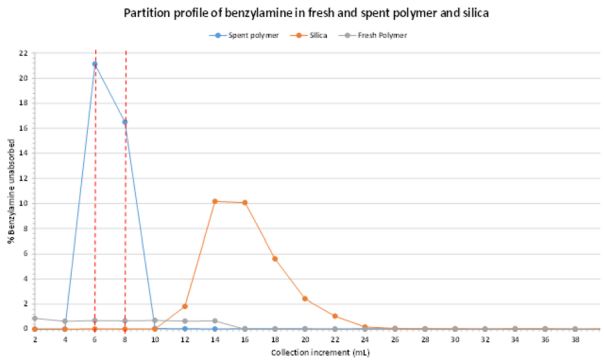

Fig. 10 Partition profile of spent **SSA-3**, **SSA-3** and silica.

a loading capacity of 0.43 mmol g^{-1} (onset of saturation, flow conditions) was determined. Batch incubation of the same column material in excess benzylamine overnight gave a mass-gain-derived loading capacity of 1.31 mmol g^{-1}. The loading capacity range of 0.43–1.31 mmol g^{-1} compares favourably to commercial polystyrene-aldehyde resins (0.4–2.0 mmol g^{-1}).

Design of experiments: optimisation of scavenging conditions. To rationalise the operational conditions for **SSA-3** in a flow context, a D-optimal design of experiments was conducted, screening solvent type (mapped using the PCA solvent space map developed by Murray and co-workers),[15] flow rate (0.1–1.0 mL min^{-1}), temperature (30–90 °C), and amine concentration (0.2–1.0 M) across 22 experiments.

To map the solvents, a representative example was selected from each quadrant of the PC1 (polarity) and PC2 (polarizability) PCA map published by Murray and co-workers (Fig. 12).[15] In addition, a centre point was also selected. The five solvents selected constituted the cuboid shape that represents a continuous space wherein the solvent can be treated as a quantitative value. The solvents chosen, were selected to be non-reactive towards aldehydes (Table 3). Due to the pseudo-continuous map, given that solvents are discreet variables, a perfect cube shape is impossible to select and is not considered necessary.[15] Given that the map was created by combining different properties and characteristics of each solvent, solvents that are grouped together in a quadrant share similar properties. This, therefore, serves as a guide towards understanding the type of solvent that is optimal for the system.

The response data (see SI) required logarithmic transformation to resolve non-normal distribution arising from a strong clustering of results at low benzylamine percentages. Following transformation, the model achieved an $R^2 = 0.98$ and $Q^2 = 0.95$ with a reproducibility of 0.99. One outlier (N2 : ACN, 90 °C, 0.1 mL min^{-1}, 0.2 M) was excluded from the final model after it was found to be statistically irresolvable, with the predicted value substantially overestimating the observed value; the exceedingly low scavenging observed under these conditions (0.02% unabsorbed) was considered anomalous and potentially artefactual.

Temperature and concentration were found to be statistically insignificant across the ranges studied and were removed from the model, indicating that **SSA-3** operates at equivalent efficiency from 30–90 °C and at amine concentrations from 0.2–1.0 M. Flow rate and its interaction with PC1 were retained in the model despite small individual coefficients, as their combined contribution was significant (see SI for more information). The two-dimensional response contour plots demonstrate that flow rate has negligible practical impact between 0.1 and 1.0 mL min^{-1} (Fig. 13 & 14).

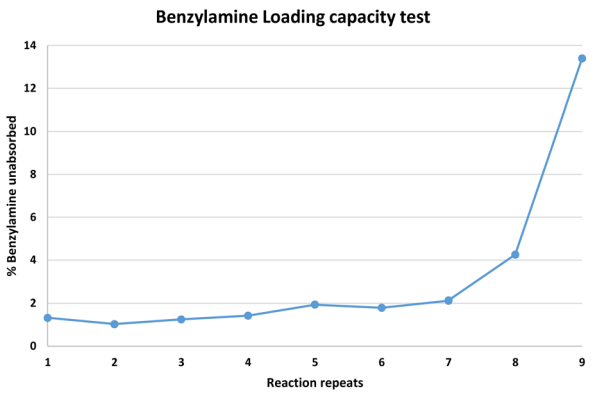

Fig. 11 Loading capacity test elution profile for **SSA-3**.

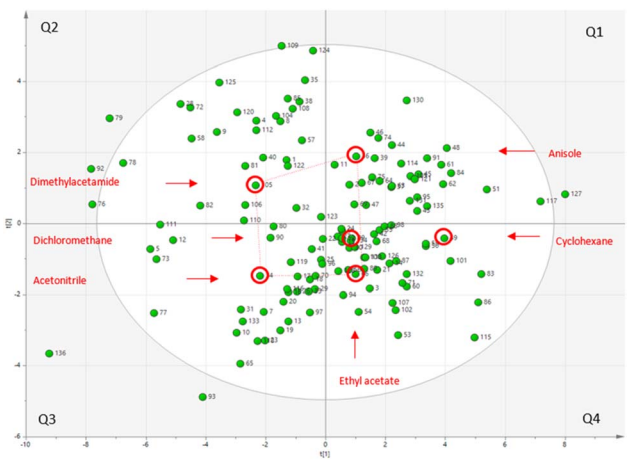

Fig. 12 Solvent map with selected solvents in each quadrant, including centre points.[15]

Table 3 Summary of combinations and respective solvents chosen

	$t[1] = -1$	$t[1] = 0$	$t[1] = +1$
$t[2] = +1$	DMA (Q2)	—	Anisole (Q1)
$t[2] = 0$	—	DCM (0,0)	CyHex (+1; 0)
$t[2] = -1$	CH_3CN (Q3)	—	EtOAc (Q4)

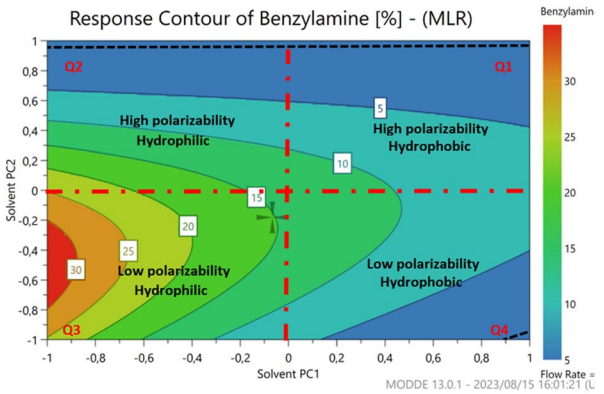

Fig. 13 Two-dimensional response contour plot at a flow rate of 1.0 mL min^{-1} with solvent PC1 and PC2 dimensions on the *x*- and *y*-axis respectively. Quadrants are indicated in red.

The absence of a significant temperature effect on scavenging efficiency is consistent with the kinetics of the imine formation. In effective solvents (EtOAc, anisole, DMA), ≥99.5% amine capture is achieved at the lowest temperature studied (30 °C) within the 20 minutes coil residence time. Pseudo-first-order kinetic analysis indicates that this requires an effective rate constant of $k \geq 0.26$ min^{-1} ($t_{1/2} \approx 2.6$ min), placing the reaction well into the kinetic saturation regime where stoichiometry rather than reaction rate governs yield. Under these conditions, the 14–50-fold rate acceleration predicted by the Arrhenius equation for an activation energy of 40–60 kJ mol^{-1} across the temperature range of 30–90 °C has no practical consequence, as there is no residual amine to capture more rapidly. For DCM and cyclohexane, which show intermediate

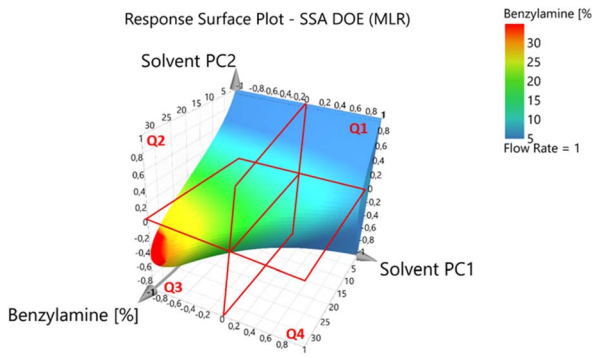

Fig. 14 Three-dimensional response contour plot at a flow rate of 1.0 mL min^{-1} with solvent PC1 and PC2 dimensions on the *x*- and *y*-axis respectively. Percentage benzylamine unabsorbed is indicated on the *z*-axis. Quadrants are indicated in red.

performance (~87%), the flat temperature response reflects the partial cancellation of two opposing effects: the rate increase is offset by the shift in the exothermic imine formation equilibrium constant with temperature. For ACN, the temperature insensitivity has a different mechanistic origin: the ~75% conversion ceiling is not a kinetic limitation as the 14–50-fold rate increase over the temperature range screened would reduce the unabsorbed fraction to below 5% if kinetics were governing. Instead a thermodynamic explanation is proposed, wherein a solvation equilibrium between ACN-coordinated amine and surface-bound imine exists that is insensitive to temperature over the range studied. Together, these observations confirm that temperature is not an operational variable requiring optimisation when deploying **SSA-3** in flow, substantially simplifying integration into continuous synthesis platforms.

Solvent dependence: Kamlet–Taft analysis and the Murray PCA framework

The dominant effect in the model was solvent type. Mapping the response surface onto the PCA solvent quadrant structure revealed that hydrophobic solvents (Q1: anisole, Q4 cyclohexane, ethyl acetate) afforded near-quantitative scavenging (<5% benzylamine unabsorbed), while Q2 solvents (dimethylacetamide — polar, polarisable) showed intermediate performance (~2–10% unabsorbed). Q3 solvents (acetonitrile — polar, non-polarisable) showed the greatest loss in scavenging efficiency (~25% unabsorbed). Dichloromethane (centre point) showed 10–15% unabsorbed amine.

The predominant influence of solvent type on scavenging efficiency was investigated further using the Kamlet–Taft linear solvation energy relationship (LSER) framework,[16,17] which parameterises solvent polarity in terms of three independent descriptors: dipolarity/polarisability (π^*), hydrogen bond donor acidity (α), and hydrogen bond acceptor basicity (β). Kamlet–Taft parameters for the six DoE solvents are summarised in Table 4, together with their mean scavenging efficiencies derived from the DoE model at centrepoint conditions (flow rate 0.55 mL min^{-1}, temperature 60 °C, concentration 0.6 M).

Simple linear regression of percentage unabsorbed amine against each Kamlet–Taft parameter individually yielded no statistically significant correlations. Regression against π^* (Fig. 15) gave $R^2 = 0.018$ ($p = 0.799$), against β gave $R^2 = 0.174$ ($p = 0.411$), and a combined $\pi^* + \beta$ model gave $R^2 = 0.198$. The failure of π^* as a predictor is apparent when inspecting the data: DMA, which has the highest π^* in the dataset (0.88), delivers near-quantitative scavenging (99.96%), while ACN, with a lower π^* of 0.75, is the worst-performing solvent at 74.9% (Fig. 15). Similarly, anisole ($\pi^* = 0.73$) and ACN ($\pi^* = 0.75$) are essentially indistinguishable by π^* yet show completely different scavenging outcomes (99.5% and 74.9% respectively). The full Kamlet–Taft LSER therefore provides no predictive framework for this dataset.

Regression against α yielded an apparently significant correlation ($R^2 = 0.727$, $p = 0.031$); however, this result arises as

Table 4 Kamlet–Taft solvatochromic parameters and scavenging performance for DoE solvents

Solvent	π*	α	β	Murray PCA quadrant	Mean % unabsorbed[a]	Mean % scavenged
ACN	0.75	0.19	0.40	PC1−/PC2−	25.1 ± 0.7	74.9
DCM	0.82	0.13	0.10	Centre	12.5 ± 2.0	87.5
Cyclohexane	0.00	0.00	0.00	PC1+/PC2 0	12.8	87.2
EtOAc	0.55	0.00	0.45	PC1+/PC2−	0.25 ± 0.24	99.8
Anisole	0.73	0.00	0.32	PC1+/PC2+	0.46 ± 0.78	99.5
DMA	0.88	0.00	0.76	PC1−/PC2+	0.041 ± 0.05	99.96

[a] Mean % unabsorbed amine (benzylamine at 5 μM) derived from DoE model-predicted values at centrepoint conditions (flow rate 0.55 mL min^{-1}, temperature 60 °C, amine concentration 0.6 M). Values ± SD shown where ≥2 replicates were available at comparable conditions. Run N2 (ACN) excluded as a statistical outlier identified by MODDE diagnostic (see text). Kamlet–Taft parameters from: Marcus, Y., *Chem. Soc. Rev.*, 1993, **22**, 409; Kamlet, M. J., Abboud, J.-L. M., Abraham, M. H. and Taft, R. W. *J. Org. Chem.*, 1983, **48**, 2877. Murray PCA quadrant assignments from: Murray, P. M. *et al.*, *Org. Biomol. Chem.*, 2016, 14, 2373. PC1 = dipolarity axis; PC2 = polarisability axis. PC1− = high dipolarity; PC1+ = low dipolarity; PC2+ = polarisable; PC2− = non-polarisable.

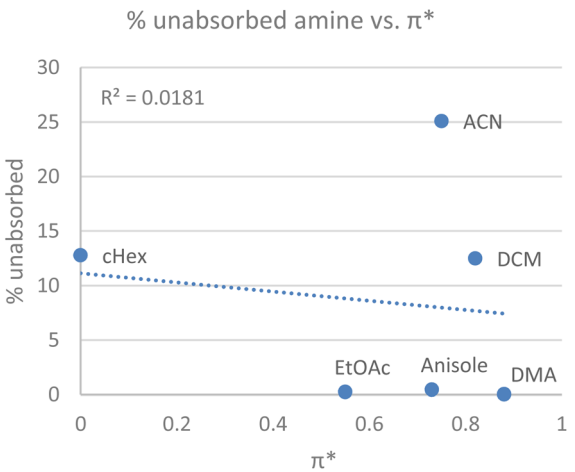

Fig. 15 Kamlet–Taft π* parameter plotted against mean % unabsorbed benzylamine for six DoE solvents ($R^2 = 0.018$, $p = 0.80$; dashed line = linear regression). No significant correlation is observed.

ACN is the only substantial HBD-active solvent in the dataset (α = 0.19) and simultaneously the worst-performing solvent. Removing ACN from the regression reduces R^2 to 0.359 and p to 0.286, confirming that the correlation has no mechanistic basis.

The failure of all single-parameter Kamlet–Taft correlations indicates that the solvent dependence cannot be described by a single physical property of the solvent and instead requires a two-dimensional description. The Murray PCA solvent classification framework,[15] provides a clearer understanding of the solvent effects (Fig. 13). The six DoE solvents occupy four distinct regions of the PCA space, their scavenging outcomes cluster in a physically interpretable pattern.

Solvents in the PC1+/PC2− (EtOAc), PC1+/PC2+ (anisole), and PC1−/PC2+ (DMA) quadrants, together with the intermediate region (DCM, cyclohexane), all deliver moderate to near-quantitative scavenging (87.2–99.96% efficiency). The sole poor-performing solvent, ACN, occupies the PC1−/PC2− quadrant, characterised by high dipolarity combined with negligible polarisability. The critical comparison is between EtOAc and ACN: both occupy the PC2− (non-polarisable) half of the map, yet EtOAc delivers 99.75% scavenging while ACN delivers only 74.9%. The distinguishing factor is PC1 : EtOAc has low dipolarity (PC1 = +1) while ACN has high dipolarity (PC1 = −1). This establishes that non-polarisability alone is insufficient to cause solvation screening — the combination of high dipolarity and low polarisability, which uniquely characterises the PC1−/PC2− quadrant, is required. A single π* value conflates these two properties and is therefore unable to resolve the EtOAc/ACN distinction.

We attribute the poor performance of ACN to a specific solvation-screening mechanism operating in polar non-polarisable solvents. We hypothesise that the rigid, strongly directional dipole of the nitrile group coordinates to the amine nitrogen through an electrostatic interaction that competes thermodynamically with surface imine formation. In polarisable solvents such as DMA and anisole, the additional dispersive interactions available through the polarisable electron cloud lower the effective solvation free energy of the amine in a way that does not compete specifically with the aldehyde surface—the amine remains available for imine formation because the polarisable solvent interacts diffusely rather than through a directed, site-specific interaction with the nitrogen lone pair. This interpretation is consistent with the observation that the temperature insensitivity of scavenging in ACN is not kinetic in origin.

Practically speaking, when deploying **SSA-3** in flow synthesis, solvents in the PC1−/PC2− quadrant of the Murray PCA map should be avoided. All other solvent classes deliver effective scavenging, and the choice among them can be made on the basis of reaction requirements, product solubility, and downstream processing considerations without concern for scavenging efficiency. This solvent-class guidance, derived from a single DoE campaign, is directly transferable to practitioners and represents a practically actionable outcome that extends beyond the characterisation of **SSA-3** itself.

Conclusions

A silica-supported aldehyde scavenger (**SSA-3**) was successfully prepared from **SBA-15** silica by a three-step sequence

Table 5 Cost comparison of commercially available amine scavengers and **SSA-3** (this work). Prices as cited in text; all SSR costs in USD per g

Product	Loading capacity (mmol g^{-1})	Cost (USD per g)	Cost (USD per mmol)
SSA-3 (this work)	0.43–1.31	1.67	1.23–3.84
Formyl polystyrene	0.4–2.0	30.44	15.25–76.14
4-Formyl phenoxyethyl PS	0.5–1.1	28.17	25.61–56.34
Methyl isocyanate PS	1.5–1.9	39.29	20.66–26.19
ScavengePore benzyl isocyanate	0.5–1.5	26.25	17.52–52.50

comprising base activation, dichloroethane alkylation, and Kornblum oxidation. The material was comprehensively characterised by FTIR, PXRD, TGA/DSC, BET physisorption, and SEM. Covalent aldehyde functionalisation was confirmed qualitatively by DNPH colorimetric test and quantitatively by loading capacity determination (0.43–1.31 mmol g^{-1}). A D-optimal DoE study established that solvent type is the sole significant variable governing scavenging efficiency across the ranges studied: hydrophobic solvents afford near-quantitative amine capture, while polar non-polarisable solvents reduce efficiency through a solvation screening mechanism. The scavenger was screened up to a back pressure of 8 bar and operates efficiently across a 10-fold range of flow rates and is insensitive to temperature (30–90 °C) and amine concentration (0.2–1.0 M), rendering it well-suited to continuous flow applications. The material cost is substantially lower (11.8 to 19.8-fold) than that of equivalent commercial polystyrene-based aldehyde resins (Table 5), with loading capacity performance within the commercial range.

SSA-3 compares favourably with commercial silica-supported aldehyde and covalent amine scavengers on the primary metrics relevant to flow chemistry deployment. The flow-derived loading capacity of 0.43–1.31 mmol g^{-1} fall within the 0.3–1.3 mmol g^{-1} range reported for commercial functionalised silica scavengers (SiliaBond series, SiliCycle Inc.). Capture kinetics under continuous flow conditions are rapid: in hydrophobic and polarisable solvents, ≥99.5% amine scavenging is achieved within the 20 minutes coil residence time at 30 °C, comparing favourably with the ≤1 h batch contact times specified for commercial silica-supported materials and substantially faster than polymer-based resins where diffusion into the polystyrene matrix is rate-limiting. The silica backbone of **SSA-3** confers the same intrinsic advantages as commercial SiliaBond materials relative to polystyrene supports: absence of solvent-induced swelling, predictable and stable packed-bed pressure drop across a broad solvent range, and thermal stability well above the operating temperatures studied here (confirmed by TGA up to 170 °C). The DoE demonstrates that scavenging performance is insensitive to flow rate (0.1–1.0 mL min^{-1}), temperature (30–90 °C), and amine concentration (0.2–1.0 M) in effective solvents, substantially simplifying operational parameter selection.

Experimental

General methods are provided in the supporting information.

Synthesis of deprotonated silica: SSA-1

Silica gel was mechanically sieved and the mesh size 90–125 mm was isolated for the synthesis. The silica (30.00 g) was refluxed in 3 M NaOH (250 mL, 3.00 M) overnight and dried *in vacuo* to yield a highly hygroscopic off-white deprotonated silica crystalline powder **SSA-1**.

Synthesis of alkylated silica: SSA-2

The deprotonated silica **SSA-1** was refluxed in pre-dried dichloroethane (250 mL) under inert conditions overnight to yield a gel-like alkylated silica product. The solvent was decanted and the gel-like product was allowed to dry and harden for 30 min. This yielded a highly hygroscopic brittle crystalline solid **SSA-2** and was stored under vacuum.

Synthesis of oxidized silica: SSA-3

The alkylated silica was crushed into a fine powder and heated in a solution of potassium carbonate (1.00 g) dissolved in dimethyl sulfoxide (250 mL) at 120 °C for 48 hours while continuously stirring. The product was vacuum filtered, washed with isopropanol and dried *in vacuo* overnight to yield oxidized silica **SSA-3** as an off-white granular powder. ν_{max}(neat)/cm^{-1} 1746 (C=O stretch, w), 1395 (C–C bend, s, broad), 1120 (Si–O–Si asymmetric stretch, m, broad), 1038 (Si–O–Si asymmetric stretch, m, broad), 881 (Si–O–Si symmetric stretching, w), 855 (Si–O–Si symmetric stretching, w), 676 (Si–O bend, w), 537 (Si–O bend, w, broad).

Synthesis of oxidized silica-DNPH: SSA-4

The DNPH solution was prepared by dissolving 2,4-dinitrophenylhydrazine (*ca* 12 g) and sulphuric acid (conc., 60 mL) in distilled water (80 mL) and diluting the solution with ethanol (96%, 200 mL) and stirring the solution overnight. Approximately 0.5 g of **SSA-3** was weighed into a flask, in triplicate. To each flask, 20 mL of the above-mentioned pre-made hydrazine solution was added and left to stir for 30 min. After the vigorous reaction and gas evolution subsided, the products were vacuum filtered and washed with ethanol to afford **SSA-4** as a dark orange granular powder (appendix F-7). ν_{max}(neat)/cm^{-1} 1739 (C=N stretch, w), 1640 (O–N=O, w), 1025 (Si–O–Si asymmetric stretching, m, broad), 955 (Si–O–Si symmetric stretching, m), 784 (Si–O–Si symmetric stretching, w, broad), 449 (Si–O, m).

Synthesis of oxidized silica-benzylated: SSA-5

To a flask of **SSA-3** (*ca* 0.5 g), 50.00 mL of a *N*-benzylamine (0.55 mL, 50.0 mmol, 1.0 M) solution was added in a single portion. The solution was stirred at room temperature for one week. The product was vacuum filtered and washed with isopropanol to afford the product **SSA-5** as an off-white granular powder. ν_{max}(-neat)/cm^{-1} 1738 (C=N stretch, m), 1645 (C–N, m), 1447 (C=C stretching, m), 1208 (Si–O–Si asymmetric stretching, m, broad), 905 (Si–O–Si symmetric stretching, m, broad), 847 (Si–O–Si symmetric stretching, w), 624 (Si–O, m, broad).

Synthesis of silica-benzylated: SSA-6

To a flask of silica (*ca* 0.5 g), 50.00 mL of a *N*-benzylamine (0.55 mL, 50.0 mmol, 1.0 M) solution was added in a single portion. The solution was stirred at room temperature for one week. The product was vacuum filtered and washed with isopropanol to afford the product **SSA-6** as a white granular powder. ν_{max}(neat)/cm^{-1} 2458 (N–H, w, broad), 1744 (N–H stretch, w), 1404 (C=C stretch, m, broad), 969 (Si–O–Si symmetric stretching, w, broad), 855 (Si–O–Si symmetric stretching, m), 600 (Si–O, w, broad).

Synthesis of silica-DNPH: SSA-7

The DNPH solution was prepared by dissolving 2,4-dinitrophenylhydrazine (*ca* 12 g) and sulphuric acid (conc., 60 mL) in distilled water (80 mL) and diluting the solution with ethanol (96%, 200 mL) and stirring the solution overnight. Approximately 0.5 g of silica was weighed into a flask. To the flask, 20 mL of the pre-made hydrazine solution was added and left to stir for 30 min. The product was vacuum filtered and washed with ethanol to afford **SSA-7** as a light-yellow powder (SI A-7). ν_{max}(neat)/cm^{-1} 1524 (O–N=O stretch, s, broad), 1180 (Si–O–Si asymmetric stretching, s, broad), 1074 (Si–O–Si asymmetric stretching, s, broad), 903 (Si–O–Si symmetric stretching, m, broad), 799 (Si–O–Si symmetric stretching, m, broad).

Loading capacity test: batch saturation

The column containing **SSA-3**, that was used in loading capacity test performed on flow, was emptied into a round bottom flask. To the **SSA-3**, a solution of *N*-benzylamine (100.00 mL, 5.00 M) in isopropanol (IPA) was added. The 5 M solution was prepared by diluting *N*-benzylamine (54.61 mL, 53.58 g, 0.5 mol) to 100 mL with IPA. The suspension was stirred gently overnight. The spent **SSA-3** was removed by vacuum filtration and washed with IPA.

Flow procedures

General procedures. All silica and silica-based reagents were used without prior swelling at a loading capacity of 0.43–1.3 mmol g^{-1} (experimentally determined). This loading capacity was assumed for reactions involving silica gel as a control for the sake of consistency. Columns were alternated according to the amount of the reagent to be scavenged (assuming the best-case scenario of all molecules being scavenged) so that the loading capacity of the scavenger was never exceeded.

Flow reactor setup: pilot flow test. The reactions were performed on a Uniqsis FlowSyn continuous flow reactor. The stock solution was injected into a PFA injection loop, 2.0 mL of sample, with the use of an Auto Loop Filler. The reactor was pre-primed with IPA. The injection loop was connected to an HPLC pump head and the reagent was pushed through the reactor with IPA. PTFE tubing (50.00 cm, 0.40 mL, 1/16″ ID) led the reagent from the injection loops to an 8.40 mL packed bed column reactor, where the reagent was allowed to partition at a flowrate of 0.28 mL min^{-1}. The column temperature was kept constant in a water bath at 30 °C. The outlet of the column was connected to the built-in pressure sensor with PTFE tubing (62.90 cm, 0.50 mL, 1/16″ ID). The mixture was then pushed through an 8 bar passive back pressure regulator connected to the pressure sensor with PTFE tubing (32.00 cm, 0.26 mL, 1/16″ ID) and thereafter collected. The collection connection volume from the collect/waste valve to the fractional collector was 0.88 mL (PTFE tubing, 110.70 cm, 0.88 mL, 1/16″ ID). The entire reaction plug was collected into a single vial, including leading and trailing edges and additional volumes of 1.00 mL pre-collect and 1.00 mL post-collect.

A standard 10.00 mm × 100.00 mm Omnifit™ glass column was used and packed so that the packed bed length was 6.20 cm for oxidized silica **SSA-3** and the mass of oxidized silica **SSA-3** was 8.0966 g resulting in a volume of 8.40 mL in IPA. The same column was used for reactions P1–P4.

The reaction mixtures were not purified further. The samples were diluted to 25.00 mL prior to analysis. The crude reaction samples were analysed with the use of quantitative liquid chromatography. The LC samples were prepared by sampling 50.00 μL of the crude reaction mixture and diluting to 1000 μL with HPLC ACN. Dilution described in detail in SI, Section A-1.7 dilution factor PDF001.

Preparation of stock solutions. Stock solution A consisted of *N*-benzylamine. These solutions were prepared by dissolving 1.09 mL *N*-benzylamine (10.00 mmol, 0.20 M) in IPA in a volumetric flask to a final volume of 50.00 mL.

Flow reactor setup: partition test. The reactions were performed on a Uniqsis FlowSyn continuous flow reactor. The stock solution was injected into a PFA injection loop, 2.0 mL of sample, with the use of an Auto Loop Filler. The reactor was pre-primed with IPA. The injection loop was connected to an HPLC pump head and the reagent was pushed through the reactor with IPA. PTFE tubing (50.00 cm, 0.40 mL, 1/16″ ID) led the reagent from the injection loops to a packed bed column reactor, where the reagent was allowed to partition at a flowrate of 0.1 mL min^{-1}. The column temperature was kept constant in a water bath at 30 °C. The outlet of the column was connected to the built-in pressure sensor with PTFE tubing (62.90 cm, 0.50 mL, 1/16″ ID).

The mixture was then pushed through an 8 bar passive back pressure regulator connected to the pressure sensor with PTFE tubing (32.00 cm, 0.26 mL, 1/16″ ID) tube and then collected. The collection connection volume from the collect/waste valve to the fractional collector was 0.88 mL (PTFE, 110.70 cm, 0.88

mL, 1/16″ ID). The entire 2.00 mL reaction plug was collected into one vial, including leading and tailing edges and additional volumes of 4.00 mL pre-collect and 8.00 mL post-collect, at 2.00 mL per vial increments.

A standard 10.00 mm × 100.00 mm glass Omnifit™ column was used and packed so that the packed bed length was 6.24 cm for oxidized silica **SSA-3** and the mass of oxidized silica **SSA-3** was 9.0032 g resulting in a volume of 8.12 mL in IPA.

This procedure was repeated with silica as a control and spent **SSA-3** as a secondary control. Due to the mass variations, the column length was kept constant.

The reaction mixtures were not purified further. The samples were evaporated and redissolved to 1.00 mL ACN prior to analysis. The crude reaction samples were analysed with the use of quantitative liquid chromatography. The LC samples were prepared by sampling 3.74 μL (20.00 μL for spent **SSA-3** and silica control) of the crude reaction mixture and diluting to 1000 μL with HPLC ACN. Dilution described in detail in SI Section A-1.7 dilution factor PDF002 and PDF016 (spent **SSA-3** and silica control).

Preparation of stock solutions. The stock solution was prepared following the same procedure described above.

Flow reactor setup: loading capacity test. The reactions were performed on a Uniqsis FlowSyn continuous flow. The stock solution was injected into a PFA injection loop, 2.0 mL of sample, with the use of an Auto Loop Filler. The reactor was pre-primed with IPA. The injection loop was connected to an HPLC pump head and the reagent was pushed through the reactor with IPA. PTFE tubing (50.00 cm, 0.40 mL, 1/16″ ID) led the reagent from the injection loops to a packed bed column reactor, where the reagent was allowed to partition at a flowrate of 0.1 mL min^{-1}. The column temperature was kept constant in a water bath at 30 °C. The outlet of the column was connected to the built-in pressure sensor with PTFE tubing (62.90 cm, 0.50 mL, 1/16″ ID).

The mixture was then pushed through an 8 bar passive back pressure regulator connected to the pressure sensor with PTFE tubing (32.00 cm, 0.26 mL PTFE, 1/16″ ID) and then collected. The collection connection volume from the collect/waste valve to the fractional collector was 0.88 mL (PTFE, 110.70 cm, 0.88 mL, 1/16″ ID). The entire 2.00 mL reaction plug was collected into one vial, including leading and tailing edges and additional volumes of 1.00 mL pre-collect and 1.00 mL post-collect, at 4.00 mL per vial increments.

The same packed bed column used for the partition test was used in this experiment. The standard 10.00 mm × 100.00 mm Omnifit™ glass column was used and packed so that the packed bed length was 6.24 cm for oxidized silica **SSA-3** and the mass of oxidized silica **SSA-3** was 9.0032 g resulting in a volume of 8.40 mL in IPA.

The reaction mixtures were not purified further. The samples were evaporated and redissolved to 1.00 mL ACN prior to analysis (vial 8 was diluted to 2.00 mL and vial 9 to 4.00 mL). The crude reaction samples were analysed with the use of quantitative liquid chromatography. The LC samples were prepared by sampling 7.46 μL (vial 8 sampled 7.46 μL and vial sampled 9 6.22 μL) of the crude reaction mixture and diluting to 1000 μL with HPLC ACN. Dilution described in detail in SI, Section A-1.7 dilution factor PDF003 (PDF004 for vial 9 and PDF005 for vial 8).

Preparation of stock solutions. The stock solution was prepared following the same procedure described above.

Flow reactor setup 1: design of experiment. For the experiments included in the DoE study, the identical flow setup was used as in the loading capacity test. Standard 10.00 mm × 100.00 mm Omnifit™ glass columns were used and packed so that the packed bed length was 4.66 ± 0.08 cm for both oxidized silica **SSA-3** and silica controls and the mass of oxidized silica **SSA-3** was kept at 4.5050 ± 0.0027 g. The column length was kept constant to ensure partitioning/scavenging path length remained constant and the mass to ensure a comparable number of active sites present for each experiment. Individual column masses are included in SI.

The reactions were performed on a Uniqsis FlowSyn continuous flow reactor. The stock solution was injected into a PFA injection loop, 2.0 mL of sample, with the use of an Auto Loop Filler. The reactor was pre-primed with the respective solvent. The injection loop was connected to a HPLC pump head and the reagent was pushed through the reactor with the respective solvent. PTFE tubing led the reagent from the injection loops to a packed bed column reactor, where the reagent was allowed to partition at a flowrate of 1.00–0.1 mL min^{-1}. The individual masses of **SSA-3** and the volumes are recorded in the SI. The column temperature was controlled with the standard fitted FlowSyn column heating module and ranged between 30–90 °C. The mixture was then pushed through an 8 bar passive back pressure regulator, to the fractional collector. The entire 2.00 mL reaction plug was collected into one vial, including leading and tailing edges and additional volumes of 1.00 mL pre-collect and 1.00 mL post-collect, at 4.00 mL per vial increments.

The reaction mixtures were not purified further. The samples were diluted prior to analysis (described in SI A-1.7). The crude reaction samples were analysed with the use of quantitative liquid chromatography. The LC samples were prepared by sampling 6.22–50.00 μL of the crude reaction mixture and diluteing to 1000 μL with HPLC ACN. Dilution described in detail in SI A, Section A-1.7 dilution factor PDF006-PDF015.

The stock solution was prepared following the same procedure described above. The same procedure was adapted for solutions of concentrations 0.60 M and 1.00 M.

Author contributions

A. Michelle Reinhardt: writing – review & editing, writing – original draft, methodology, investigation, formal analysis, data curation, conceptualization. Jenny-Lee Panayides: writing – review & editing, writing – original draft, supervision, project administration, funding acquisition. Darren L. Riley: writing – review & editing, writing – original draft, supervision, project administration, funding acquisition.

Conflicts of interest

The authors declare that they have no known competing financial interests or personal relationships that could have appeared to influence the work reported in this paper.

Data availability

The data supporting this article have been included as part of the supplementary information (SI). Supplementary information: quantitative LC, BET, TGA, DSC, PXRD, SEM and IR characterisation data, and DoE raw data and graphs. See DOI: https://doi.org/10.1039/d6ra04582k.

Acknowledgements

This work was supported by the National Research Foundation (NRF) of South Africa (grant numbers PMDS22063029267 and SRUG190329425006), the University of Pretoria (Research and Development Program), and the Council for Scientific and Industrial Research (CSIR), South Africa. Opinions expressed in this publication are those of the authors and are not necessarily attributed to the NRF. The authors acknowledge University of Pretoria Laboratory for Microscopy and Microanalysis. We would also like to thank Prof Liezel van der Merwe, Dr Fredrick Malan, Prof N. Manyala and Dr Bakhoum from the University of Pretoria for their contributions in physical and chemical characterization.

References

1 I. R. Baxendale and S. V Ley, in *New Avenues to Efficient Chemical Synthesis*, ed. P. H. Seeberger and T. Blume, Springer Berlin Heidelberg, Berlin, Heidelberg, 2007, pp. 151–185.
2 C. Blackburn, B. Guan, P. Fleming, K. Shiosaki and S. Tsai, *Tetrahedron Lett.*, 1998, **39**, 3635–3638.
3 S. W. Kaldor, M. G. Siegel, J. E. Fritz, B. A. Dressman and P. J. Hahn, *Tetrahedron Lett.*, 1996, **37**, 7193–7196.
4 E. A. Pascual-Alfonso Carmen and M. J. Carlos, *Synlett*, 2000, **2000**, 205–208.
5 M. W. Creswell, G. L. Bolton, J. C. Hodges and M. Meppen, *Tetrahedron*, 1998, **54**, 3983–3998.
6 T. R. Ryder, L.-Y. Hu, M. F. Rafferty, E. Millerman, B. G. Szoke and K. Tarczy-Hornoch, *Bioorg. Med. Chem. Lett.*, 1999, **9**, 1813–1818.
7 M. T. Fiorini and C. Abell, *Tetrahedron Lett.*, 1998, **39**, 1827–1830.
8 J. Gorzynski Smith, *Organic Chemistry*, McGraw-Hill, Singapore, 4th edn, 2014.
9 M. Panunzio, M. Villa, A. Missio, T. Rossi and P. Seneci, *Tetrahedron Lett.*, 1998, **39**, 6585–6588.
10 S. E. Ault-Justus, J. C. Hodges and M. W. Wilson, *Biotechnol. Bioeng.*, 1998, **61**, 17–22.
11 A. Itoh, T. Miura and N. Tada, in *Comprehensive Organic Synthesis*, ed. P. Knochel, Elsevier, Amsterdam, 2014, Second Edition, pp. 744–769.
12 P. K. Jal, S. Patel and B. K. Mishra, *Talanta*, 2004, **62**, 1005–1028.
13 M. Muñoz, D. Flores, G. Morillo, R. Narváez, A. Marcilla and M. Rosero, *Sustainable Chem.*, 2025, **6**, 42.
14 R. Huirache-Acuña, R. Nava, C. Peza-Ledesma, J. Lara-Romero, G. Alonso-Núez, B. Pawelec and E. Rivera-Muñoz, *Materials*, 2013, **6**, 4139–4167.
15 P. M. Murray, T. D. Sheppard, F. Bellany, L. Benhamou, D.-K. Bučar and A. B. Tabor, *Org. Biomol. Chem.*, 2016, **14**, 2373.
16 Y. Marcus, *Chem. Soc. Rev.*, 1993, **22**, 409.
17 M. J. Kamlet, J. L. M. Abboud, M. H. Abraham and R. W. Taft, *J. Org. Chem.*, 1983, **48**, 2877–2887.